Carbohydrate Polymers 87 (2012) 2012–2018

Contents lists available at SciVerse ScienceDirect

Carbohydrate Polymers

journal homepage: www.elsevier.com/locate/carbpol

Structure and properties of regenerated cellulose fibers from different technology processes

Guansen Jiang[a], Weifeng Huang[a], Lin Li[b], Xiao Wang[a], Fengjian Pang[b], Yumei Zhang[a,*], Huaping Wang[a]

[a] State Key Laboratory for Modification of Chemical Fibers and Polymer Materials, Donghua University, Shanghai 201620, China
[b] Shandong Helon Co., Ltd, Shandong 261000, China

ARTICLE INFO

Article history:
Received 30 March 2011
Received in revised form
29 September 2011
Accepted 5 October 2011
Available online 25 October 2011

Keywords:
Cellulose fiber
Structure
Synchrotron radiation
Technology process

ABSTRACT

The crystalline and microstructure of the regenerated cellulose fibers prepared from different solvents and technology processes were investigated by synchrotron wide-angle X-ray diffraction (WAXD) and small-angle X-ray scattering (SAXS). WAXD results indicated that the crystal orientation, crystallinity of Lyocell and IL-cell fibers were higher than those of Viscose and Newdal fibers. The size of micro-voids located in the cross-section of regenerated cellulose fibers was analyzed based on the results of SAXS. And the technology process had little effect on the radius of the micro-voids. The micro-voids in Viscose and Newdal fibers have longer length (L) and greater misorientation (B_Φ) than that in Lyocell and IL-cell fibers. This reveals that the average void volumes of Viscose and Newdal fibers were larger. Furthermore, the regenerated cellulose fibers from dry-jet-wet-spinning process exhibited completely a higher E-modulus, tenacity than the fibers spun by wet-spinning method did.

1. Introduction

Polymers from renewable resources have attracted much attention because of their biodegradability and potential to replace petrochemicals in many fields. Cellulose as a linear polysaccharide exhibited outstanding properties and wide applications, and became the most abundant renewable polymeric material.

However, processing of cellulose is difficult in general as this natural polymer does not melt or solve in usual solvents due to its inter- and intra-hydrogen bond, partially crystalline structure. Moreover, the traditional Viscose technologies to produce cellulose-regenerated materials caused serious environmental burdens. Therefore, new processing approaches have long been scrutinized to avoid complicated processing routes and hazardous byproducts (Fink, Weigel, Purz, & Ganster, 2001).

It is found that cellulose can swell and dissolve in several solvents, such as N-methylmorpholine-N-oxide (NMMO) (Fink et al., 2001), dimethyl sulfoxide (DMSO)/paraformaldehyde (PF), N, N-dimethylacetamide (DMAc)/lithium chloride (LiCl) and alkali solutions (Roy, Budtova, & Navard, 2003) and ionic liquids (ILs) (Swatloski, Spear, Holbrey, & Rogers, 2002). Among those solvents mentioned above, only the use of NMMO/H_2O in its process of commercialization has made technical breakthroughs and lead to a new man-made cellulose fibers with the generic name, Lyocell (Fink et al., 2001).

Swatloski et al. (2002) first reported that ILs could be used as another direct solvent for cellulose without derivatization, which disclosed another new solvent for cellulose following NMMO/H_2O. Since then, numbers of ILs dissolving cellulose have been found (Fukaya, Hayashi, Wada, & Ohno, 2008; Fukaya, Sugimoto, & Ohno, 2006; Zhang, Wu, Zhang, & He, 2005). The dissolving ability and mechanism, the solution properties and the processing ability related to cellulose and ILs have been reported (Kosan, Michels, & Meister, 2008; Kosan, Schwikal, & Meister, 2010; Moulthrop, Swatloski, Moyna, & Rogers, 2005; Remsing, Swatloski, Rogers, & Moyna, 2006; Youngs, Hardacre, & Holbrey, 2007; Youngs et al., 2006; Zhang et al., 2005, 2010). Besides, the cellulose could also be dissolved in ILs with other material formed the composite (Kadokawa, Murakami, Takegawa, & Kaneko, 2009; Murakami, Kaneko, & Kadokawa, 2007; Takegawa, Murakami, Kaneko, & Kadokawa, 2010; Zhang et al., 2007). As the unique advantage of ionic liquid in environment and specific chemical–physical properties, the potential industrial applications of ILs were developed.

The preparation of regenerated cellulose fibers through direct dissolution not only overcome the tedious technology for producing conventional Viscose fibers, but also exhibited a series of unique performance (Kosan et al., 2008). The mechanical properties of

* Corresponding author. Tel.: +86 021 67792957; fax: +86 021 67792855.
E-mail addresses: jgs115@126.com (G. Jiang), yellow11bee@163.com (W. Huang), lilin3285@163.com (L. Li), wxmelora@163.com (X. Wang), pangfj@163169.net (F. Pang), zhangym@dhu.edu.cn (Y. Zhang), wanghp@dhu.edu.cn (H. Wang).

0144-8617/$ – see front matter © 2011 Elsevier Ltd. All rights reserved.
doi:10.1016/j.carbpol.2011.10.022

regenerated cellulose fibers vary according to processing technologies (Kosan et al., 2008). Compared with the Viscose fibers (Fink et al., 2001), for example, the regenerated cellulose fibers prepared from the direct dissolution technology showed larger tenacity and modulus and lower elongation. It is known that the mechanical properties depend on the micro-morphology structure which is influenced by the processing technology. Although the mechanical properties of regenerated cellulose fibers from different technology have been reported, the details of the relationship between the properties and structure need further research.

In this article, the regenerated cellulose fibers were prepared from the traditional and modified Viscose technology, NMMO and ILs technology, respectively. The morphology and structure of the regenerated cellulose fibers, including the surface and cross-section morphology, the orientation of the chain, the crystalline structure and the micro-voids, are discussed to explain the relationship between the structure and mechanical properties of the cellulose fibers.

2. Experimental

2.1. Materials

The Viscose, Newdal, Lyocell and IL-cell fibers were spun from different technology processes, which include the traditional and modified Viscose process, NMMO and ILs process.

Viscose (Helon®, Shandong Helon Co. Ltd., China), was spun with a conventional wet-spinning process from cellulose pulp (degree of polymerization (*DP*): 450–550, Shandong Helon Co. Ltd., China).

Newdal (Newdal®, Shandong Helon Co. Ltd., China) is the high wet modulus fiber, supplied by Shandong Helon Co. Ltd., China, which was spun with a modified Viscose process from cellulose pulp (*DP*: 600–900, Shandong Helon Co. Ltd., China).

Lyocell (Tencel®, Lenzing Group, Austria), was spun with a dry-jet-wet-spinning process from cellulose pulp (*DP*: 500–900, Lenzing Group, Austria) with NMMO as solvent.

IL-cell, prepared in Shandong Helon Co. Ltd., China, was spun with a dry-jet-wet-spinning process from cellulose pulp (*DP*: 500–800, Shandong Helon Co. Ltd., China) with 1-N-butyl-3-methylimidazolium chloride ([BMIM]Cl) as solvent and water as coagulating bath.

2.2. Measurements

Wide-angle X-ray diffraction (WAXD) experiments were carried out at the Beam line (U7B) in the National Synchrotron Radiation Laboratory (NSRL) with a wavelength of 0.154 nm. A bundle of cellulose fibers were placed in a sample holder with the fiber direction perpendicular to the X-ray beam. The distance between the image plate (Mar 345) and the sample for WAXD was 213.5 mm. A typical image acquisition time was 180 s.

The 2D WAXD pattern was processed with the software package FIT2D (Hammersley, 1987–1997) to correct for air scattering.

The crystal orientation along the fiber axis was calculated by the Herman's orientation parameter (f_c) (Klug & Alexamder, 1954):

$$f_c = \frac{(3\langle\cos^2\varphi_{c,Z}\rangle - 1)}{2} \quad (1)$$

The orientation parameter $\langle\cos^2\varphi_{c,Z}\rangle$ was determined according to the Wilchinsky Model (1959) and crystal symmetry of regenerated cellulose fibers (Kolpak & Blackwell, 1976) with the characteristic reflections in equatorial, (1 1 0), (0 2 0) and ($\bar{1}$ 1 0). For the reflections ($h\,k\,l$), the orientation parameter $\langle\cos^2\varphi_{h\,k\,l}\rangle$ can be calculated from equation (Klug & Alexamder, 1954):

$$\langle\cos^2\varphi_{h\,k\,l}\rangle = \frac{\int_0^{\pi/2} I(\varphi_{h\,k\,l})\cos^2\varphi_{h\,k\,l}\sin\varphi_{h\,k\,l}d\varphi_{h\,k\,l}}{\int_0^{\pi/2} I(\varphi_{h\,k\,l})\sin\varphi_{h\,k\,l}d\varphi_{h\,k\,l}} \quad (2)$$

where $\varphi_{h\,k\,l}$ represents the azimuthal angle and $I(\varphi_{h\,k\,l})$ is the intensity along the ($h\,k\,l$) reflection.

The orientation parameter $\langle\cos^2\varphi_{h\,k\,l}\rangle$ of regenerated cellulose was evaluated from WAXD 2D detector images according to the method reported in the literature (Gindl, Martinschitz, Boesecke, & Keckes, 2006).

The crystallinity of regenerated cellulose was quantified from the WAXD pattern using the following procedures. On the basis of the 2D WAXD patterns of powder samples, which were corrected for air scattering, the integrated diffraction intensity profile was calculated. And from the curve-fitting process of this profile, the data were analyzed with Peak fit software (version 4.12, Seasolve Co., San Jose, CA). Then, the crystallinity was calculated according to Eq. (3):

$$W_{c,x} = \frac{I_c}{I_c + I_a} \times 100\% \quad (3)$$

where $W_{c,x}$ is the crystallinity, I_c and I_a are the total crystal peak area of the crystalline and the amorphous phases, respectively.

The average crystallite size $L_{h\,k\,l}$ perpendicular to the reflection planes ($h\,k\,l$) was determined according to the Scherrer's equation:

$$L_{h\,k\,l} = \frac{K\lambda}{B_{h\,k\,l}\cos\theta} \quad (4)$$

where λ is the wavelength of the X-rays, θ is half of the diffraction angle (2θ), $B_{h\,k\,l}$ is the half-width of reflection plane ($h\,k\,l$) and K is a constant that is commonly assigned a value of 0.9.

Birefringence measurements of fibers were carried out on an Olympus Co. (Tokyo, Japan) XP51 optical polarized light microscope with the aid of an Olympus CTB Berek compensator. Moreover the birefringence of regenerated cellulose fibers were calculated from the empirical equation as follows:

$$\Delta n = \frac{\theta\lambda}{180^\circ d} \quad (5)$$

where $\lambda = 0.589 \times 10^{-9}$ m; θ is the compensatory angle (°); d is the diameter of cellulose filament.

SAXS profiles were obtained at Beamline (16B1) in Shanghai Synchrotron Radiation Facility (SSRF). The wavelength used was 0.124 nm. A CCD X-ray detector (MAR CCD 165) was employed at a distance of 5053 mm from the sample. Tendon of ox (L = 65.0 nm) was used for calibration. A method of ionization chamber reading was used to subtract the background scattering from the air pathway and instrumentation. The corresponding profiles were normalized to beam intensity and corrected relative to an empty sample cell background. A typical image acquisition time was 40 s. The images were carried out using the software package FIT2D (Hammersley, 1987–1997).

For the regenerated cellulose fibers, it is known for us that the contribution for SAXS is mainly from the micro-voids due to the solution spinning process (Chen et al., 2006, 2007; Crawshaw & Cameron, 2000; Moss, Butler, Müller, & Cameron, 2002; Statton, 1956; Vickers, Briggs, Ibbett, Payne, & Smith, 2001). As the schematic diagram for the drawn cellulose fibers is illustrated in Fig. 2, the needle-shaped micro-voids and aligned parallel to the fiber direction caused a streak along the equator in SAXS. The radius of micro-voids with circles cross section can be described by Guinier

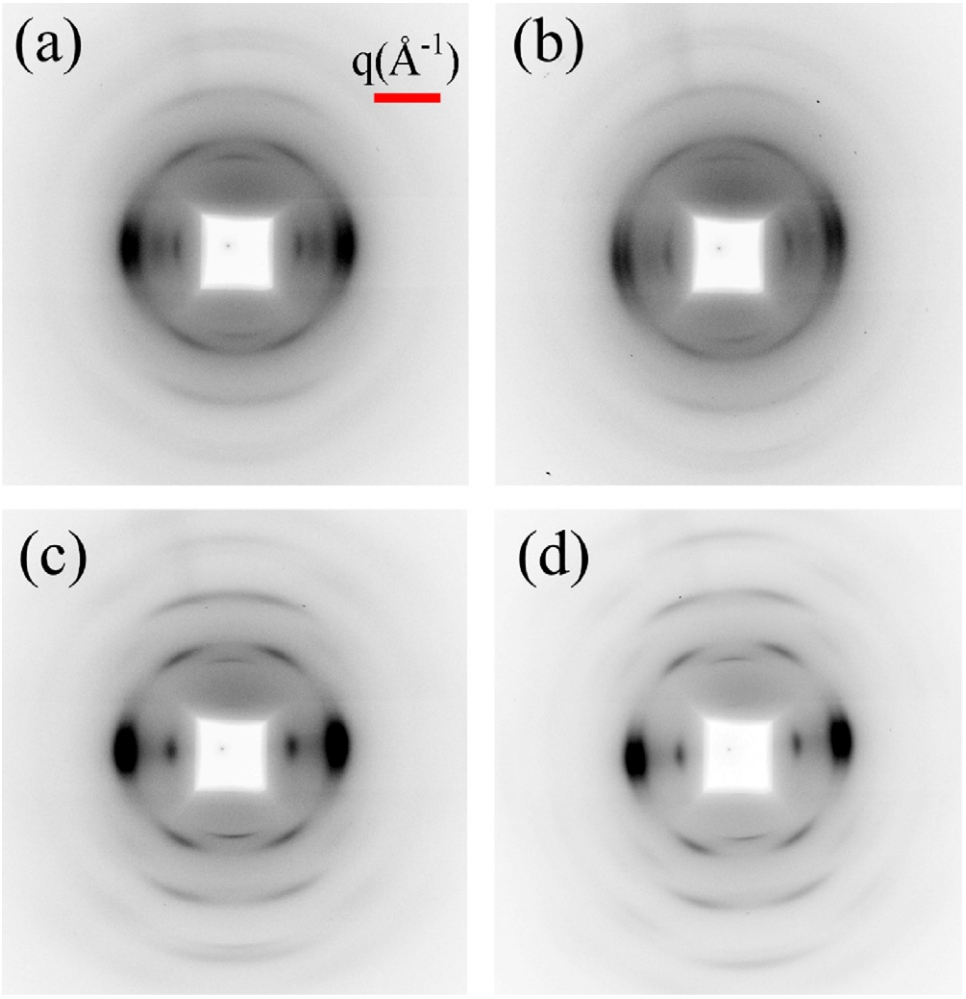

Fig. 1. WAXD patterns of the regenerated cellulose fibers from different technology processes: (a) Viscose fiber, (b) Newdal fiber, (c) Lyocell fiber, and (d) IL-cell fiber.

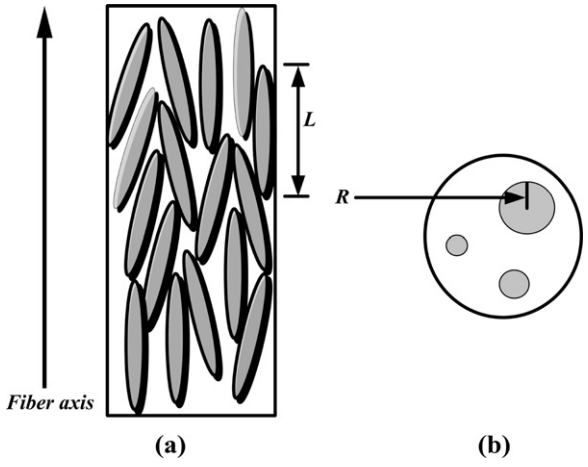

Fig. 2. Schematic diagram of the micro-void in the orientated fiber: (a) parallel to the fibers axis and (b) perpendicular to the fiber axis. The parameter R is the average radius of the voids in cross-section after the method of Guinier for the oriented needle-shape scattering moieties. The misorientation B_Φ and the length L of the voids parallel to the fiber axis were estimated from azimuthal scans of the data using the method of Ruland.

functions, the $\ln(I)$ as a function of q^2 can be given by Eq. (6) (Guinier & Fournet, 1955):

$$I(q) = I(0)\exp\left(\frac{-q^2R^2}{5}\right) \tag{6}$$

where R is the radius of micro-voids with circles cross section, q ($q = 4\pi\sin\theta/\lambda$) is the scattering vector, 2θ is the scattering angle and λ is the wavelength. Guinier plot of the scattered intensities along the layer line in the horizontal direction, which shown a typical polydisperse system, and an analysis for these results can be made by resolving the curve into successive tangents (Fischer, Herchenroder, Manley, & Stamm, 1978; Statton, 1956). Subsequently, the sizes of the voids in cross-section of regenerated cellulose fibers were calculated by Eq. (6).

The average length and the misorientation orientation of micro-voids from the fiber axis were calculated based on the method of Ruland (1969). Many authors (Chen et al., 2006, 2007; Ran et al., 2001; Vickers et al., 2001) have determined the angular spread (B_{obs}) of each azimuthal profile as a function of s ($s = 2\sin\theta/\lambda$). With the regenerated cellulose fibers, it is found that the azimuthal scans of the equatorial streak at different scattering vectors can be described by the Lorentzian/Cauchy-type functions. Simultaneity, from these angular spread, the micro-voids length (L) and the

Table 1
The physical properties of regenerated cellulose fibers from different technology processes.

Sample	Viscose	Newdal	Lyocell	IL-cell
Linear density (dtex)[a]	1.32	1.32	1.32	2.22
Fiber-*DP*	300	350	550	540
E-modulus (0.5–0.9%) (cN/dtex)	35.7	46.9	88.3	75.1
Elongation (%)	22.6	22.6	13.1	7.24
Tenacity (dry) (cN/dtex)[b]	2.15	2.84	4.29	3.54
Tenacity (wet) (cN/dtex)	1.41	1.70	2.75	2.59
Moisture regain (%)	13	13	11	11

[a] 1 dtex = 0.1 g/km.
[b] 1 cN = 0.01 N.

misorientation width (B_Φ) can be calculated from the following equation:

$$sB_{obs} = \frac{1}{L} + sB_\Phi \quad \text{Cauchy-Cauchy} \tag{7}$$

where B_{obs} is actually the full width at half maximum of the azimuthal profile from the equatorial streak fitted with a Lorentzian function; $s = 2\sin\theta/\lambda$, where 2θ represents the scattering angle and λ is X-ray wavelength.

All samples for SEM experiments were treated with absolute alcohol and then stored at a constant humidity (60%) and temperature (room temperature) for 2 days. The surfaces of samples were treated by sputter gold before the testing. The surface of the regenerated cellulose fibers was observed by using a Hitachi S-3000N scanning electron microscope.

The cross-sections of a bundle of regenerated cellulose fibers cutting by slicer were observed under the microscope Model as XSZ-360AP made by Shanghai Weitu Instruments Technology Development Co. Ltd.

Mechanical tests were carried out with material testing equipment (XQ-1, China) at least ten standard tensile specimens were tested for each series. The drawing speed was 20 mm/min. The specimens were stored at a constant temperature (room temperature) for 2 days before the testing. The wet tenacity of fiber steeped in distilled water at 25 °C for 3 min were measured.

The moisture regain of regenerated cellulose fibers were determined from Eq. (8):

$$w = \frac{g - g_c}{g_c} \times 100\% \tag{8}$$

where w is the moisture regain; g is the wet weight of fibers; g_c is the dry weight of fibers.

The degree of polymerization of regenerated cellulose fibers were estimated by the standard procedure of measuring the intrinsic viscosity $[\eta]$ in Cuoxam solution by using the empirical relation of $DP_{\text{Cuoxam}} = 2\,[\eta]_{\text{Cuoxam}}$ (Kosan et al., 2008).

3. Results and discussion

3.1. Mechanical properties of regenerated cellulose fibers from different technology processes

The mechanical properties of regenerated cellulose fibers from different technology processes were shown in Table 1. The mechanical properties of regenerated cellulose varied greatly with the different technology processes. The most remarkable thing lies in the two different methods of spinning, wet spinning and dry-jet-wet-spinning. As shown in Table 1, the regenerated cellulose fibers from dry-jet-wet-spinning exhibited higher tenacity and modulus as well as lower elongation. Before the discussion of different results, it should be pointed that higher average molecular weight usually leads to higher tensile strengths and modulus for the regenerated cellulose fibers prepared from the similar technology process. Therefore, the tenacity of the Viscose fibers and Newdal fibers from wet-spinning technology were lower as a result of the lower molecular weight of pulp. Because the conventional Viscose fiber was subject to the oldest technology and method, the cellulose pulp with lower *DP* would be more appropriate to produce the regenerated cellulose fibers. By comparison, the higher *DP* cellulose pulp can be dissolved by direct dissolution method, which is one of the advantages of this technology. For Viscose and Newdal fibers, the similar *DP* but different technology processes were applied. In comparison with Viscose fibers, the tenacity and modulus of Newdal fibers were enhanced due to the modification of the coagulation conditions and multiple drawing. As is shown in Figs. 3 and 4, the modified Viscose technology made the Newdal fibers presented smoother surfaces and more uniform cross-sections than Viscose fibers.

For the Lyocell and IL-cell fibers from dry-jet-wet-spinning, Lyocell fibers with the similar *DP* exhibited a higher E-modulus, tenacity and elongation. Superficially, the mechanical properties of Lyocell fibers have apparently precedence over IL-cell fibers. However, what must be emphasized here that the pure water of the coagulation bath was applied during producing IL-cell fibers although in general much milder coagulation condition with a certain contents of solvent is always applied to make the fiber uniform and dense. In fact, from Figs. 3 and 4, the surfaces and cross-sections of the Lyocell and IL-cell fibers were smooth and uniform, which is in agreement with previous studies (Cao et al., 2009; Fink et al., 2001). It was suggested that the mechanical properties of regenerated cellulose fibers from ILs could be improved (Fink et al., 2001) if the spinning conditions were optimized further.

3.2. Crystalline structure and orientation of regenerated cellulose fibers from different technology processes

The crystalline structure of regenerated cellulose fibers from different technologies was studied by WAXD. The WAXD patterns were shown in Fig. 1. By calculating the interplanar spacing, all the reflections can be indexed based on the unit cell parameters $a = 8.10$ Å (1 Å = 0.1 nm), $b = 9.03$ Å, $c = 10.31$ Å, and $\gamma = 117.18°$ determined by Langan, Nishiyama, and Chanzy (2001). It is clear that all the regenerated cellulose fibers showed the typical cellulose II crystalline structure with a monoclinic unit cell. The characteristic reflections ($\bar{1}\,1\,0$), (1 1 0) and (0 2 0) are located on the equator and the (0 0 2) reflection is located in meridian while the non-($h\,k\,0$) reflections are located at the off-axis positions, which indicates that the crystalline structure was preferred to orient along the fiber axis. The formation of the crystalline phase of cellulose fibers during the regeneration process was independent on the technology process. However, the width, length and intensity of the reflection arc are different from the technology process. In the WAXD patterns of Viscose (Fig. 1(a)) and Newdal (Fig. 1(b)) fibers, reflections appeared as broad arcs, suggesting the relatively low crystal orientation. While in the patterns of Lyocell (Fig. 1(c)) and IL-cell (Fig. 1(d)) fibers, narrower reflection arcs, especially in equator, were observed, indicating a higher degree of crystal orientation.

The crystallinity and crystal size were determined by corresponding peak separation analysis. On the basis of the cellulose II structure, six significant reflection peaks and an amorphous peak were chosen to fit the experimental data. The crystal size and crystallinity of all samples were given in Table 2. Obviously, the crystallinity of Lyocell and IL-cell fibers are higher than the values of Viscose and Newdal fibers. Meanwhile, the degree of crystal orientation as well as the birefringence (shown in Table 2) of Lyocell and IL-cell fibers is apparently higher than that of the Viscose and Newdal fibers. There is no doubt that the dry-jet-wet-spinning process has positive action to the orientation and crystallization of the cellulose chain. It is also reasonable for us to deduce that the

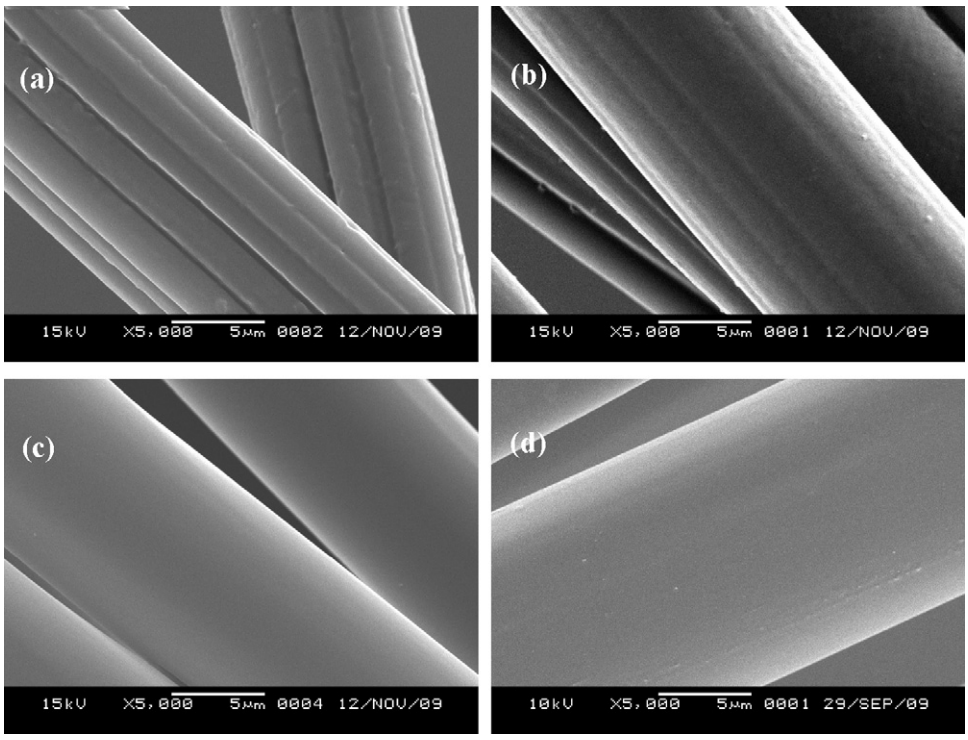

Fig. 3. Scanning electron microscopy photographs of surface of the regenerated cellulose fibers from different technology processes: (a) Viscose fiber, (b) Newdal fiber, (c) Lyocell fiber, and (d) IL-cell fiber.

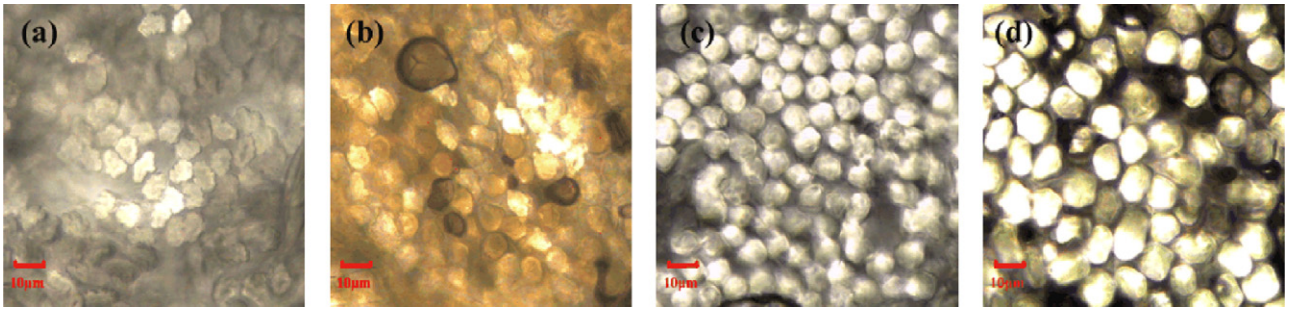

Fig. 4. Microscopy photographs of cross-section of regenerated cellulose fibers from different technology processes: (a) Viscose fiber, (b) Newdal fiber, (c) Lyocell fiber, and (d) IL-cell fiber.

Table 2
Crystal size, crystallinity, degree of crystal orientation (f_c), and birefringence (Δn) of the regenerated cellulose fibers from different technology processes.

Sample	Crystal size (Å)						Crystallinity (%)	Crystal orientation f_c (%)	Birefringence $\Delta n \times 10^2$
	$\bar{1}10$	002	110	012	020	103			
Viscose	37.5	37.8	38.3	37.4	38.3	38.1	68	94	2.55
Newdal	39.5	39.2	39.1	39.3	38.6	38.8	65	93	2.51
Lyocell	35.8	35.2	35.5	34.4	34.2	35.4	73	96	2.88
IL-cell	36.5	36.2	36.0	35.4	35.3	35.6	74	98	2.85

crystallinity and degree of crystal orientation contributed significantly to the increase of strength and modulus, and decrease of elongation of regenerated cellulose fibers from dry-jet-wet-spinning process due to remarkable contribution of the effective orientation of macromolecular chain during extrusion and coagulation process.

The crystal sizes of Viscose and Newdal fibers spun form wet spinning are somewhat larger. Although the crystal of greater size could contribute to the total crystallinity of semicrystalline polymers, it has less effect on the strength and modulus of regenerated cellulose fibers during stretching. The smaller crystal size in Lyocell fiber is more favorable for enhancing the strength and modulus of regenerated cellulose fibers as well as the elongation.

3.3. Micromorphology of regenerated cellulose fibers from different technology processes

For cellulose fibers, many studies (Crawshaw & Cameron, 2000; Chen et al., 2006, 2007; Statton, 1956; Vickers et al., 2001) have suggested that the elongated equatorial streak in the SAXS, for both dry and wet regenerated cellulose fibers, was assigned as the scattering by long thin voids and parallel to the fiber axis. The meridional

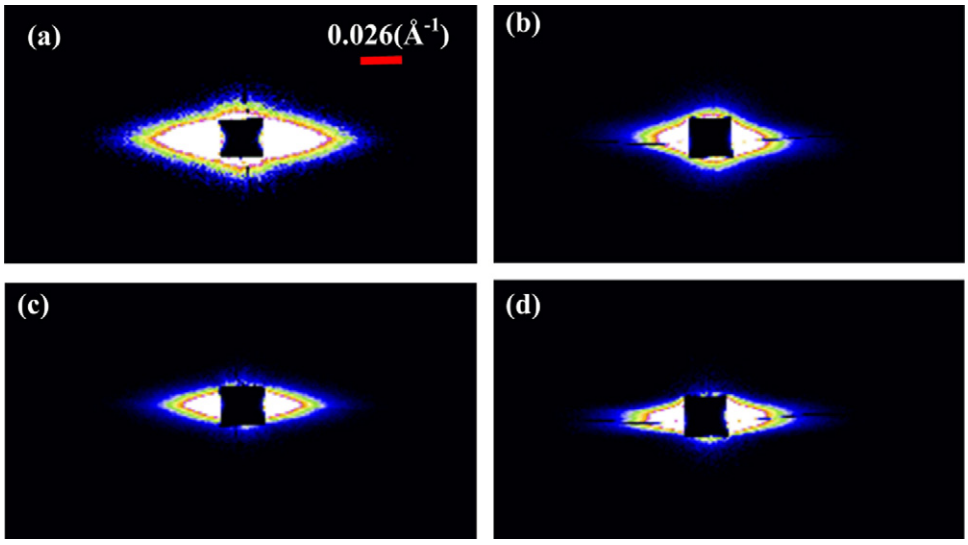

Fig. 5. SAXS patterns of the regenerated cellulose fibers from different technology processes: (a) Viscose fiber, (b) Newdal fiber, (c) Lyocell fiber, and (d) IL-cell fiber.

Table 3
Different sizes of the voids in cross-section, micro-voids length, and misorientation of the regenerated cellulose fibers from different technology processes.

Sample	R_1 (Å)	R_2 (Å)	R_3 (Å)	Micro-voids length L (Å)	Misorientation B_Φ (°)
Viscose	16.7	38.1	–	13,200	37
Newdal	16.4	33.5	59.0	3700	26
Lyocell	16.5	33.3	53.8	2500	20
IL-cell	15.2	33.0	66.1	3330	13

broadening in the cellulose fibers was accounted for increasing misorientation of the voids and a reduction in void length (Ruland, 1969; Wang, Ruland, & Cohen, 1993).

Fig. 5 presents the SAXS patterns of regenerated cellulose fibers from different technology processes. As the common feature, it can be clearly seen that the scattering patterns exhibits a sharp and elongated equatorial streak in intensity due to the needle-shaped micro-voids and aligned parallel to the fiber direction. In addition, the Lyocell (Fig. 5(c)) and IL-cell fibers (Fig. 5(d)) show a more sharp streak along the equator than Viscose (Fig. 5(a)) and Newdal fibers (Fig. 5(b)). The SAXS pattern of Viscose fibers (Fig. 5(a)) shows stronger scattering intensity than other three samples, suggesting that there are more micro-voids exist in Viscose fibers compared to other regenerated cellulose fibers. The calculation was conducted to illustrate the results of the micro-voids in the regenerated cellulose fibers from different technology processes.

According to Eq. (6), the radius of micro-voids in cross-section of regenerated cellulose fibers were calculated and the results are listed in Table 3. It indicated the size of micro-voids in the cross-section of the regenerated cellulose fiber exhibited multi-order characters always with approximately 16 Å, 33 Å and 60 Å. It is suggested that the technology process had little effect on the radius of the micro-voids in the regenerated cellulose fibers.

Furthermore, the angular spread (B_{obs}) of each azimuthal profile as a function of s plotted according to Ruland method and the micro-voids length (L) and the misorientation width (B_Φ) were calculated (shown in Table 3).

From Table 3, the Viscose and Newdal fibers show the higher values of the misorientation. In contrast, the values of misorientation of Lyocell and IL-cell fibers are lower, which is consistent with earlier results obtained from WAXD (Fig. 1). Moreover, for the Viscose and Newdal fibers, the micro-voids length are obviously longer than that of Lyocell and IL-cell fibers, indicating that the average void volume fraction of the Viscose and Newdal fibers are higher than that of Lyocell and IL-cell fibers. Especially, it is suggested that the average void volume fraction is the major factor to cause the decrease of strength and modulus of regenerated cellulose fibers with similar crystallinity and degree of crystal orientation, such as Viscose and Newdal fibers. However, compared to the Viscose and Newdal fibers, the Lyocell and IL-cell fibers have a shorter micro-voids and smaller misorientation, implying that homogeneous structure could provide regenerated cellulose fibers with more excellent performances.

4. Conclusions

The structure and properties of regenerated cellulose fibers prepared from different technology processes (the Viscose, Newdal, Lyocell and IL-cell fibers) were comparatively studied. The Lyocell and IL-cell fibers had a higher degree of crystal orientation and total crystallinity. The micro-voids length and misorientation degree of Lyocell and IL-cell fibers were lower. Thus, result in the surface shape and cross-section of fibers is regular and well-proportioned, and the fibers presented strong tear strength and initial modulus. By contrast, the Viscose and Newdal fibers exhibited a lower degree of crystal orientation and total crystallinity, and the higher length of micro-voids and misorientation degree, which meant the larger average volume of the micro-voids and defect consist in the fiber. The results of the comparative study indicated that the NMMO and ILs are expected to be much more efficient and flexible in cellulose dissolution and shaping processes.

Acknowledgements

The work is supported by a grant from National Natural Science Foundation of China (50873025), and the innovation funds for Ph.D. students (Jiang Guansen) of Donghua University.

Appendix A. Supplementary data

Supplementary data associated with this article can be found, in the online version, at doi:10.1016/j.carbpol.2011.10.022.

References

Cao, Y., Wu, J., Zhang, J., Li, H. Q., Zhang, Y. & He, J. S. (2009). Room temperature ionic liquids (RTIL): A new and versatile platform for cellulose processing and derivatization. *Chemical Engineering Journal*, *147*, 13–21.

Chen, X. M., Burger, C., Fang, D. F., Ruan, D., Zhang, L. N., Hsiao, B. S., et al. (2006). X-ray studies of regenerated cellulose fibers wet spun from cotton linter pulp in NaOH/thiourea aqueous solutions. *Polymer*, *47*, 2839–2848.

Chen, X. M., Burger, C., Wan, F., Zhang, J., Rong, L. X., Hsiao, B. S., et al. (2007). Structure study of cellulose fibers wet-spun from environmentally friendly NaOH/Urea aqueous solutions. *Biomacromolecules*, *8*, 1918–1926.

Crawshaw, J. & Cameron, R. E. (2000). A small angle X-ray scattering study of pore structure in Tencel cellulose fibres and the effects of physical treatments. *Polymer*, *41*, 4691–4698.

Fink, H. P., Weigel, P., Purz, H. J. & Ganster, J. (2001). Structure formation of regenerated cellulose materials from NMMO-solutions. *Progress in Polymer Science*, *26*, 1473–1524.

Fischer, E. W., Herchenroder, P., Manley, R. S. J. & Stamm, M. (1978). Small-angle neutron scattering of selectively deuterated cellulose. *Macromolecules*, *11*, 213–217.

Fukaya, Y., Hayashi, K., Wada, M. & Ohno, H. (2008). Cellulose dissolution with polar ionic liquids under mild conditions: Required factors for anions. *Green Chemistry*, *10*, 44–46.

Fukaya, Y., Sugimoto, A. & Ohno, H. (2006). Superior solubility of polysaccharides in low viscosity, polar, and halogen-free 1,3-bialkyl-imidazolium formats. *Biomacromolecules*, *7*, 3295–3297.

Gindl, W., Martinschitz, K. J., Boesecke, P. & Keckes, J. (2006). Orientation of cellulose crystallites in regenerated cellulose fibres under tensile and bending loads. *Cellulose*, *13*, 621–627.

Guinier, A. & Fournet, G. (1955). *Small-angle scattering of X-rays*. New York: Wiley.

Hammersley (1987–1997). A FIT2D 2-D detector calibration/correction; file reformatting; 2-D fitting; European Synchrotron Radiation Facility (ESRF).

Kadokawa, J., Murakami, M., Takegawa, A. & Kaneko, Y. (2009). Preparation of cellulose-starch composite gel and fibrous material from a mixture of the polysaccharides in ionic liquid. *Carbohydrate Polymers*, *75*, 180–183.

Klug, H. & Alexamder, L. (1954). *X-ray diffraction procedures*. New York: John Wiley & Sons.

Kolpak, F. J. & Blackwell, J. (1976). Determination of the structure of cellulose II. *Macromolecules*, *9*, 273–278.

Kosan, B., Michels, V. & Meister, F. (2008). Dissolution and forming of cellulose with ionic liquids. *Cellulose*, *15*, 59–66.

Kosan, B., Schwikal, K. & Meister, F. (2010). Solution states of cellulose in selected direct dissolution agents. *Cellulose*, *17*, 495–506.

Langan, P., Nishiyama, Y. & Chanzy, H. (2001). X-ray structure of mercerized cellulose II at 1 Å resolution. *Biomacromolecules*, *2*, 410–416.

Moulthrop, J. S., Swatloski, R. P., Moyna, G. & Rogers, R. D. (2005). High-resolution ^{13}C NMR studies of cellulose and cellulose oligomers in ionic liquid solutions. *Chemical Communications*, *12*, 1557–1559.

Moss, C. E., Butler, M. F., Müller, M. & Cameron, R. E. (2002). Microfocus small-angle X-ray scattering investigation of the skin-core microstructure of Lyocell cellulose fibers. *Journal of Applied Polymer Science*, *83*, 2799–2816.

Murakami, M., Kaneko, Y. & Kadokawa, J. (2007). Preparation of cellulose polymerized ionic liquid composite by in-situ polymerization of polymerizable ionic liquid in cellulose-dissolving solution. *Carbohydrate Polymers*, *69*, 378–381.

Ran, S., Fang, D., Zong, X., Hsiao, B. S., Chu, B. & Cunniff, P. M. (2001). Structural changes during deformation of Kevlar fibers via on-line synchrotron SAXS/WAXD techniques. *Polymer*, *42*, 1601–1612.

Remsing, R. C., Swatloski, R. P., Rogers, R. D. & Moyna, G. (2006). Mechanism of cellulose dissolution in the ionic liquid 1-N-Butyl-3-methylimidazolium chloride: A ^{13}C and $^{35/37}Cl$ NMR relaxation study on model systems. *Chemical Communications*, *12*, 1271–1273.

Roy, C., Budtova, T. & Navard, P. (2003). Rheological properties and gelation of aqueous cellulose-NaOH solutions. *Biomacromolecules*, *4*, 259–264.

Ruland, W. (1969). Small-angle scattering studies on carbonized cellulose fibers. *Journal of Polymer Science Part C Polymer Symposium*, *28*(1), 143–151.

Statton, W. O. (1956). Crystallite regularity and void content in cellulose fibers as shown by small-angle X-ray scattering. *Journal of Polymer Science*, *22*, 385–397.

Swatloski, R. P., Spear, S. K., Holbrey, J. D. & Rogers, R. D. (2002). Dissolution of cellulose with ionic liquids. *Journal of the American Chemical Society*, *124*, 4974–4975.

Takegawa, A., Murakami, M., Kaneko, Y. & Kadokawa, J. (2010). Preparation of chitin/cellulose composite gels and films with ionic liquids. *Carbohydrate Polymers*, *79*, 85–90.

Vickers, M. E., Briggs, N. P., Ibbett, R. N., Payne, J. J. & Smith, S. B. (2001). Small angle X-ray scattering studies on Lyocell cellulosic fiber: The effects of drying, re-wetting and changing coagulation temperature. *Polymer*, *42*, 8241–8248.

Wang, W., Ruland, W. & Cohen, Y. (1993). Fibrillar and microfibrillar structures in poly (p-phenylene terephthalamide) fibers. *Acta Polymerica*, *44*, 273–278.

Wilchinsky, Z. W. (1959). Advance in X-ray analysis. *Journal of Applied Physics*, *30*, 782–789.

Youngs, T. G. A., Hardacre, C. & Holbrey, J. D. (2007). Glucose solvation by the ionic liquid 1, 3-dimethylimidazolium chloride: A simulation study. *The Journal of Physical Chemistry B*, *111*, 13765–13774.

Youngs, T. G. A., Holbrey, J. D., Deetlefs, M., Nieuwenhuyzen, M., Gomes, M. F. C. & Hardacre, C. (2006). A molecular dynamics study of glucose solvation in the ionic liquid 1, 3-dimethylimidazolium chloride. *Chemphyschem*, *7*, 2279–2281.

Zhang, H., Wang, Z. G., Zhang, Z. N., Wu, J., Zhang, J. & He, J. S. (2007). Regenerated-cellulose/multiwalled-carbon-nanotube composite fibers with enhanced mechanical properties prepared with the ionic liquid 1-Allyl-3-methylimidazolium chloride. *Advanced Materials*, *19*, 698–704.

Zhang, H., Wu, J., Zhang, J. & He, J. S. (2005). 1-Allyl-3-methylimidazolium chloride room temperature ionic liquid: A new and powerful nonderivatizing solvent for cellulose. *Macromolecules*, *38*, 8272–8277.

Zhang, J. M., Zhang, H., Wu, J., Zhang, J., He, J. S. & Xiang, J. F. (2010). NMR spectroscopic studies of cellobiose solvation in EMIMAc aimed to understand the dissolution mechanism of cellulose in ionic liquids. *Physical Chemistry Chemical Physics*, *12*, 1941–1947.